Journal of Power Sources 230 (2013) 76–80

Contents lists available at SciVerse ScienceDirect

Journal of Power Sources

journal homepage: www.elsevier.com/locate/jpowsour

Short communication

Li-rich layered composite $Li[Li_{0.2}Ni_{0.2}Mn_{0.6}]O_2$ synthesized by a novel approach as cathode material for lithium ion battery

Jing Lin [a], Daobin Mu [a,*], Ying Jin [b], Borong Wu [a], Yunfeng Ma [a], Feng Wu [a]

[a] Beijing Key Laboratory of Environmental Science and Engineering, School of Chemical Engineering and Environment, Beijing Institute of Technology, Beijing 100081, China
[b] National Center for Materials Service Safety, University of Science and Technology Beijing, Beijing 100083, China

HIGHLIGHTS

- Li-rich layered composite $Li[Li_{0.2}Ni_{0.2}Mn_{0.6}]O_2$ is synthesized by a novel approach.
- Carbon felt is used to control the particles growth and simplify the preparation.
- The composite exhibits high reversible capacity and excellent cycling stability.
- First-principles calculation is performed to identify the crystalline structure.

ARTICLE INFO

Article history:
Received 18 October 2012
Received in revised form
26 November 2012
Accepted 8 December 2012
Available online 20 December 2012

Keywords:
Li-rich
Layer structure
Cathode material
Carbon felt
Lithium ion battery

ABSTRACT

Li-rich layered composite $Li[Li_{0.2}Ni_{0.2}Mn_{0.6}]O_2$ is prepared by a novel approach in which carbon felt acts as a carrier for synthesis reaction. The as-prepared material is characterized by SEM, ICP and XRD, its electrochemical performance is also examined with galvanostatic charge/discharge and CV measurements. It is showed that the facile process controls effectively the particle growth (in size around 100–200 nm) of the composite and its chemical composition. The as-prepared material shows a high initial discharge capacity about 288 mAh g^{-1} when charged to 4.8 V, and a retained value of 246.8 mAh g^{-1} in the 40th cycle. The crystalline structure of the composite is simulated further by Material Studio. It is revealed that the composite has a compatible layer structure merged by Li_2MnO_3 and $LiNi_{0.5}Mn_{0.5}O_2$, which makes substantial contribution to the cycleability of the electrode. In addition, the lithiation/delithiaion properties including charge transfer resistance and lithium ion diffusion coefficient are studied with electrochemical impedance spectra.

1. Introduction

As electric vehicles develop rapidly, high energy density, long cycle life and excellent thermal stability become the requirements for the next generation of lithium ion battery. Cathode material plays an important role in the electrochemical performance of lithium ion battery and contributes approximately 40% to the price of a cell [1]. Recently, more and more interests have been focused on the series of Li-rich cathode materials because of their high capacity [2–8].

However, several problems still obstruct the commercial application of the promising $xLi_2MnO_3\cdot(1-x)LiNi_{0.5}Mn_{0.5}O_2$ cathode materials. Firstly, the charge mechanism at high voltage plateau above 4.5 V is not well clarified. Meanwhile, large irreversible capacity loss in the first cycle seriously restricts its development as well [9,10]. Especially, the performance of this kind of materials is closely related to its structure which is influenced heavily by synthesis conditions. Therefore, much attention is paid to the fabrication and optimization of the material with co-precipitation method, sol–gel method, etc [11–15]. As we know, the optimized electrochemical performance reported is that the initial discharge capacity at 0.1 C generally locates in the range of 250–280 mAh g^{-1}, the retained discharge capacity is about 200–240 mA h g^{-1} after 40 cycles [12,16–18]. This study proposes a novel approach to controllably prepare Li-rich layered composite with the aim of realizing a facile synthesis of high capacity cathode materials for lithium ion battery.

The novel synthesis process was investigated to fabricate the Li-rich layered composite $Li[Li_{0.2}Ni_{0.2}Mn_{0.6}]O_2$, i.e., $xLi_2MnO_3\cdot(1-x)LiNi_{0.5}Mn_{0.5}O_2$ ($x = 0.6$), in which carbon felt acted as the carrier of solution using its porous structure to control the growth of composite particles in combination with selected calcination

* Corresponding author. Tel.: +86 10 68918770; fax: +86 10 68918828.
E-mail address: mudb@bit.edu.cn (D. Mu).

0378-7753/$ – see front matter © 2012 Elsevier B.V. All rights reserved.
http://dx.doi.org/10.1016/j.jpowsour.2012.12.042

treatment. Characterizations were conducted to examine the morphology, chemical composition and crystalline structure of the composite material. Material Studio software was adopted to simulate the composite structure so as to discuss its effect on electrode property in-depth. The electrochemical performance of the cathode was studied as well.

2. Experimental

2.1. A novel synthesis for composite $Li[Li_{0.2}Ni_{0.2}Mn_{0.6}]O_2$

A certain amount of $LiNO_3$ (Shanghai Aladdin, GR), $Mn(NO_3)_2$ (Shanghai Aladdin, 50 wt.%, AR) and $Ni(NO_3)_2{\cdot}6H_2O$ (Shanghai Aladdin, 99%, GR) were dissolved in distilled water according to the element ratio of $Li[Li_{0.2}Ni_{0.2}Mn_{0.6}]O_2$ to form nitrate solution. Citric acid (Shanghai Aladdin, 99.5%, AR) was added to the solution under continuous stirring for 12 h. The molar ratio of (Li + Mn + Ni):$C_6H_8O_7{\cdot}H_2O$ is 1:1. Then, the mixed solution was adsorbed by carbon felt (Jiangsu TongKang) with S_{BET} of 1281 $m^2\ g^{-1}$ and dried at 80 °C in an oven until the formation of a fluffy precursor. The precursor was decomposed at 350 °C for 10 h in air and calcinated subsequently at 900 °C for 4 h in air. Finally, the products were obtained after being slowly cooled to room temperature at a cooling rate of 5 °C min^{-1}.

2.2. Material characterization

The morphology of the synthesized material was observed by field emission scanning electron microscope (FE-SEM, S-4800, Hitachi) with an accelerating voltage of 15 kV. The thermal decomposition behavior of the precursor was examined by thermogravimetry (TG) and differential thermal analysis (DTA) using SEIKO TG/DTA6300 at a ramping rate of 10 °C min^{-1} in air. The chemical composition of the sample was analyzed by inductively coupled plasma (ICP, SPECTRO ARCOS EOP, SPECTRO Analytical Instruments GmbH) measurement. The powder X-ray diffraction (XRD, UltimaIV-185, Rigaku) measurement using Cu-Kα radiation was employed to characterize the crystalline structure of the material. XRD data were acquired with a step size of 0.02° from 10 to 70°, the acquisition step time of 0.0025 min. The source tension and current are 40 kV and 40 mA, respectively. The simulation of the crystalline structure was performed on the Material Studio platform.

2.3. Electrochemical performance

Electrochemical tests were conducted on CR2025-type coin cell. The procedure to fabricate the cathode was as follows: 80 wt.% Li $[Li_{0.2}Ni_{0.2}Mn_{0.6}]O_2$, 10 wt.% Super P and 10 wt.% polyvinylidene fluoride (PVDF) in N-methyl pyrrolidinone (NMP) solvent were mixed and ground to form a homogeneous slurry. The slurry was then spread onto an aluminium foil current collector and dried at 80 °C in oven. With lithium sheet as the counter electrode, Celgard2300 film as the separator, the cells were assembled with an electrolyte of 1 M $LiPF_6$ in a mixture of ethylene carbonate (EC)/dimethyl carbonate (DEC) (1:1 volume ratio of EC:DEC) in an argon-filled glove box where both moisture and oxygen contents were less than 1 ppm. Charge/discharge performance was tested by LAND CT2001A battery testing system at a current density of 20 mA g^{-1} (0.1 C rate) and a voltage range of 2.0 V–4.8 V. Cyclic voltammetry (CV) curves were recorded from 2 V to 5 V at a scan rate of 0.1 mV s^{-1}. Electrochemical impedance spectroscopy (EIS) measurement was performed in a frequency range of 100 kHz–10 mHz with a signal amplitude of 5 mV. The impedance spectra of the cathodes at different state of charge (SOC) were measured. The applied voltages were 3 V (open-circuit), 4 V (during charging) and 4.8 V (after charging) respectively. All of the CV and EIS measurements were carried out on CHI600C electrochemical workstation. The voltages mentioned in the paper were referred to Li^+/Li redox couple.

3. Results and discussion

It is inferred that the meshed micro-porous carbon felt adsorbs a large number of solution as carrier by comparing the images of Fig. 1(a) and (b). It will also provide reaction sites before being burned up to obtain the final composite. Besides the precursor treatment, the calcination is also crucial to the formation of the composite. Fig. 2 gives TG/DTA curves of the precursor in the temperature range from 40 °C to 900 °C. The small weight-loss is mainly associated with the loss of adsorbed water and crystal water from $Ni(NO_3)_2{\cdot}6H_2O$ and $C_6H_8O_7{\cdot}H_2O$, accompanying an exothermic peak of the precursor at 180 °C. The obvious weight-loss corresponding to large exothermic peak appears between 300 °C and 350 °C due to the formation of preliminary particles, which helps determining the pre-treatment temperature. The related reactions may be assigned to the decomposition of the complexing agent and the crystallization of solid solution phases. With the calcination treatment at 900 °C, fine crystal particles smaller than 200 nm in size are obtained, as seen in Fig. 1(c). The crystallite size calculated from XRD data is in the range of 80–100 nm which is smaller than the particle size observed from SEM image. It is also shown that the as-prepared $Li[Li_{0.2}Ni_{0.2}Mn_{0.6}]O_2$ particles have uniform crystal morphology, which can promote sufficient contact of the oxide material to the electrolyte allowing then a large surface area to proceed electrochemical reaction. The composition of the as-prepared composite is listed in Table 1. The element contents in the practical formula are almost the same as that in the nominal formula $Li[Li_{0.2}Ni_{0.2}Mn_{0.6}]O_2$. It is clear that the particle growth with no aggregation is controlled effectively by the novel approach as well as the chemical composition.

XRD pattern of $LiNi_{0.5}Mn_{0.5}O_2$ is calculated based on the physical parameters of space group $R\bar{3}m$ and cell parameters $a = 2.897$ Å and $c = 14.31$ Å [19] using Reflex module of Material Studio, as shown in Fig. 3. The measured XRD characteristic peaks of the as-prepared $Li[Li_{0.2}Ni_{0.2}Mn_{0.6}]O_2$ i.e., $xLi_2MnO_3{\cdot}(1-x)LiNi_{0.5}Mn_{0.5}O_2$ ($x = 0.6$) are similar to the simulated XRD pattern of $LiNi_{0.5}Mn_{0.5}O_2$. It indicates that the composite has the α-$NaFeO_2$ layer structure. But there still appear some peaks around 22–25° in the measured XRD pattern, as many reports pointed out [9,11], they are relevant to the $LiMn_6$ cation ordering that occurs in the transition metal layers of Li_2MnO_3, and can be indexed to the Li_2MnO_3 (JCPDS Card No. 27-1252) with monoclinic unit cell and space group C2/m. On the other hand, the lattice parameters of the composite are calculated as $a = 2.8522$ Å and $c = 14.2236$ Å from the measured XRD pattern by a least squares method with an assumption of $R\bar{3}m$ structure. The high c/a ratio of 4.9869 (greater than 4.899) implies an explicit layer structure. Furthermore, the divergence of lattice parameter indicates the phase transition which can be attributed to the formation of solid solution phase consisting of Li_2MnO_3 and $LiNi_{0.5}Mn_{0.5}O_2$. The sharp splits in (006)/(102) and (108)/(110) peaks further identify the layer structure of the as-prepared material and the good structural compatibility between Li_2MnO_3 and $LiNi_{0.5}Mn_{0.5}O_2$ [20]. In addition, it is indicated that the material has a low level of Li^+ and Ni^{2+} disordering because the I_{003}/I_{104} ratio of 1.4881 is greater than 1.2. It is also confirmed that a well-ordered structure is obtained in the composite according to the low $(I_{006} + I_{102})/I_{101}$ ratio of 0.3465. Thus, the composite structure may benefit the reversible insertion/extraction of lithium ion through the two-dimension channel built by MO_6 [21,22], leading to the enhancement of cycling performance.

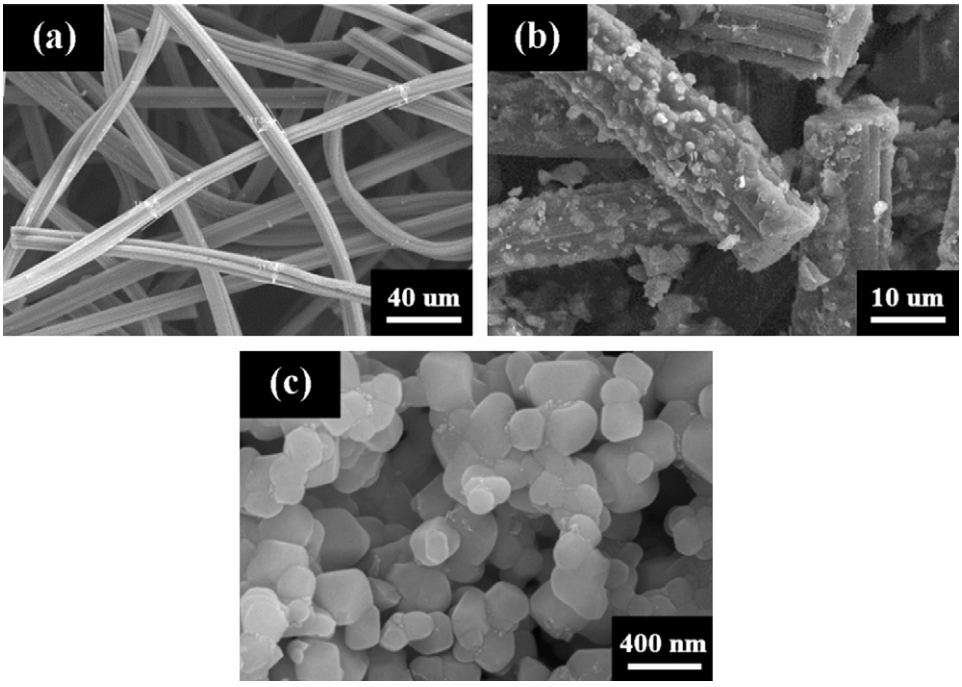

Fig. 1. SEM images of (a) carbon felt; (b) the precursor; (c) $Li[Li_{0.2}Ni_{0.2}Mn_{0.6}]O_2$ particles.

Fig. 4 illustrates the cycling performance of the cathode cycled between 2.0 V and 4.8 V at a current density of 20 mA g^{-1}. It is seen that the initial charge/discharge capacities are significantly higher than the ones in subsequent cycles. The $LiNi_{0.5}Mn_{0.5}O_2$ component holds 160.3 mAh g^{-1} of the total initial charge capacity, while the Li_2MnO_3 component activated above 4.5 V contributes 177 mAh g^{-1}, as seen in Fig. 5. The discharge capacity reaches 288.6 mAh g^{-1} in the first cycle, showing a steady decrease with an average loss of 1.045 mAh g^{-1} per cycle. It still keeps the value of 246.8 mAh g^{-1} in the 40th cycle with a capacity retention ratio of 86%. The cathode also exhibits a coulombic efficiency of 96.4% after 40 cycles.

To clarify the cycling stability further, the crystalline structure of the as-prepared $Li[Li_{0.2}Ni_{0.2}Mn_{0.6}]O_2$ is analyzed with the simulation based on the lattice parameters obtained from the measured XRD data and the atom occupied positions (Li : 3a (0, 0, 0); Li, Mn and Ni : 3b (0, 0, 0.5); O : 6c (0, 0, 0.25)) [23]. The computed result is shown in Fig. 6 to present a schematic of layered-structure built by lithium layers and mixed layers of transition metal and lithium. In the simulated structure of $Li[Li_{0.2}Ni_{0.2}Mn_{0.6}]O_2$, the lithium layers are located above and below the mixed layers of transition metal and lithium. The manganese, nickel and part of lithium atoms occupy all the octahedral sites of the mixed layers, the oxygen atoms at the apices of the octahedra are represented by small black

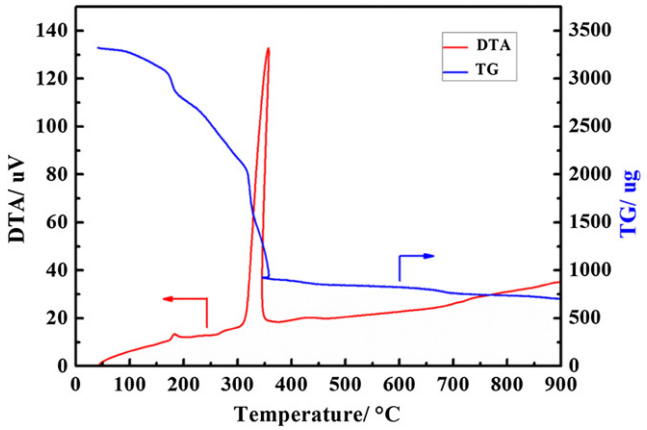

Fig. 2. TG/DTA curves of the precursor.

Table 1
Chemical composition of the as-prepared material.

	Element ratio in mole				Chemical formula
	Li	Ni	Mn	O	
Designed	1.200	0.200	0.600	2.000	$Li[Li_{0.2}Ni_{0.2}Mn_{0.6}]O_2$
Measured	1.218	0.200	0.586	2.000	$Li_{1.218}Ni_{0.2}Mn_{0.586}O_2$

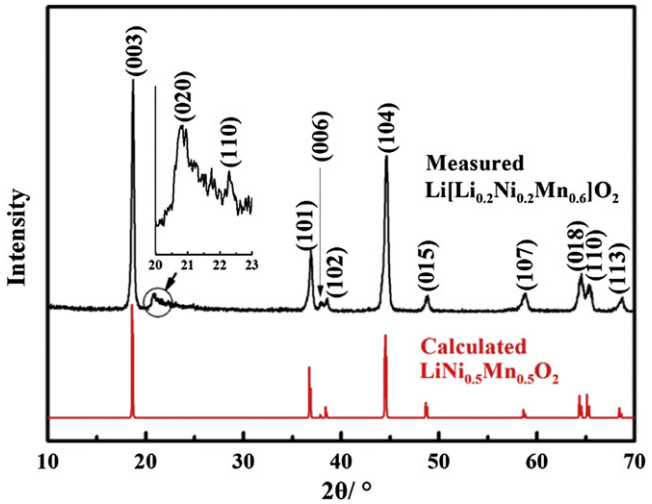

Fig. 3. Calculated XRD pattern of $LiNi_{0.5}Mn_{0.5}O_2$ and measured XRD pattern of the as-prepared $Li[Li_{0.2}Ni_{0.2}Mn_{0.6}]O_2$.

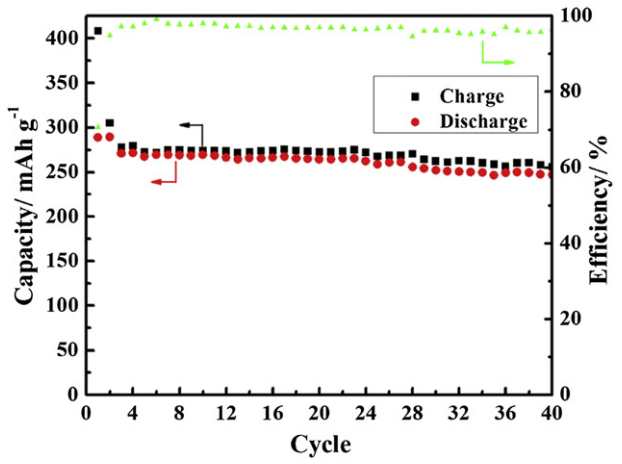

Fig. 4. Cycling performance of the as-prepared material $Li[Li_{0.2}Ni_{0.2}Mn_{0.6}]O_2$ cycled between 2.0 V and 4.8 V at a current density of 20 mA g^{-1}.

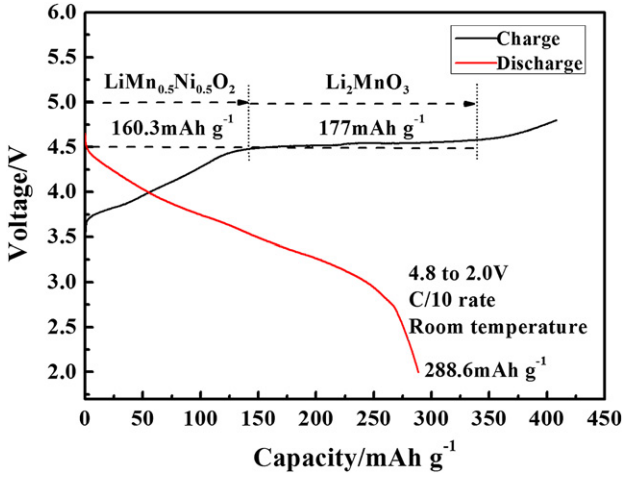

Fig. 5. Charge/discharge curves of the as-prepared material $Li[Li_{0.2}Ni_{0.2}Mn_{0.6}]O_2$ in the first cycle.

dots. The excess lithium in the mixed layers will fill the vacancy of lithium, substantially stabilizing the composite structure during the charge/discharge process [9,24]. Thereby the stable layered-structure contributes greatly to the excellent cycling performance of the cathode.

As shown in Fig. 7, electrochemical impedance spectra (EIS) of the $Li[Li_{0.2}Ni_{0.2}Mn_{0.6}]O_2$ cathodes at different SOC are investigated to get insight into the electrochemical process during the first charge. The EIS plot under open-circuit voltage consists of a semicircle related to the charge-transfer process in high frequency region and a straight line corresponding to Warburg diffusion process in low frequency region [25]. While the plot under 4 V includes two semicircles, the one near the lower frequency region is suggested to associate with the delithiation reaction. The appearance of semicircle in the high frequency range carries information on the solid electrolyte interphase (SEI) [26], which happens after the system is stabilized. Under 4.8 V, it is shown that the semicircle size in the high frequency region becomes larger in the plot. These Nyquist plots are fitted with the equivalent electrical circuit (EEC) in Fig. 7, where R_s stands for solution resistance, R_{sf} and CPE_1 represent the resistance and the capacitance of SEI film. R_{ct} and CPE_2 correspond to charge-transfer resistance and capacitance. Z_w is the Warburg impedance related to lithium ions diffusion [27]. According to the fitted results obtained by software Zsimpwin, the charge transfer resistance R_{ct} decreases slightly from 126.2 Ω under open-circuit voltage 3 V to 124.7 Ω under 4 V. The cyclic voltammetry (Fig. 8) result indicates that the oxidation of Ni^{2+} to Ni^{4+} happens at 3.6 V–3.9 V during the first charge cycle, so the decrease of R_{ct} under 4 V is thought owing to the electrochemical reaction. When the cathode is charged to 4.8 V, the charge transfer resistance R_{ct} increases to 227.8 Ω. It may be ascribed to either the passivation effect of MnO_2 on the electrode surface or the structural rearrangements of the $Li[Li_{0.2}Ni_{0.2}Mn_{0.6}]O_2$ composite due to oxygen loss from its lattice [28]. As reported in literature [29], electron removal from O^{2-} species at the surface will accompany Li^+ extraction at 4.5 V because the Fermi level is situated within the oxygen valence band under such a high voltage. As a result, oxygen evolution occurs with the oxidation of O^{2-}.

The diffusion coefficient, D_{Li^+}, can be calculated in terms of the following equation [30],

$$D_{Li^+} = \frac{0.5R^2T^2}{c^2F^4A^2\sigma^2}$$

Where R is the gas constant, T the absolute temperature, c the concentration of Li^+ in the material, F the Faraday constant, A the surface area of the electrode, and σ the Warburg factor obeying the following relationship,

$$Z_{re} = \sigma\omega^{-1/2}$$

Z_{re} is the real part of impedance, thus σ can be obtained from the linear fitting of Z_{re} vs. $\omega^{-1/2}$ in the medium–low frequency range. As a result, the diffusion coefficient of the as-prepared material before charging is 2.49×10^{-16} cm^2 s^{-1}, it is slightly smaller than the value of 4.71×10^{-16} cm^2 s^{-1} obtained under 4.8 V. It is clear

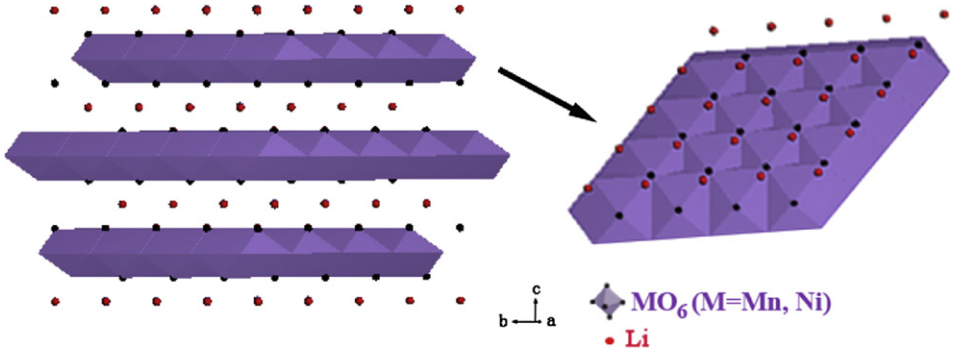

Fig. 6. Schematic diagram of simulated crystal structure of the as-prepared composite $Li[Li_{0.2}Ni_{0.2}Mn_{0.6}]O_2$ (Li_2MnO_3 merged with $Li[Ni_{0.5}Mn_{0.5}]O_2$).

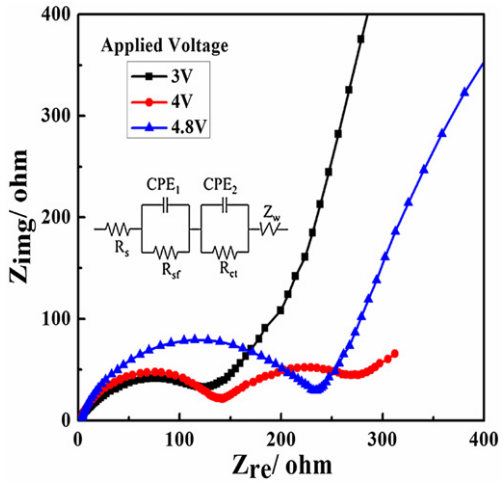

Fig. 7. Nyquist plots of $Li[Li_{0.2}Ni_{0.2}Mn_{0.6}]O_2$ cathode at different state of charge.

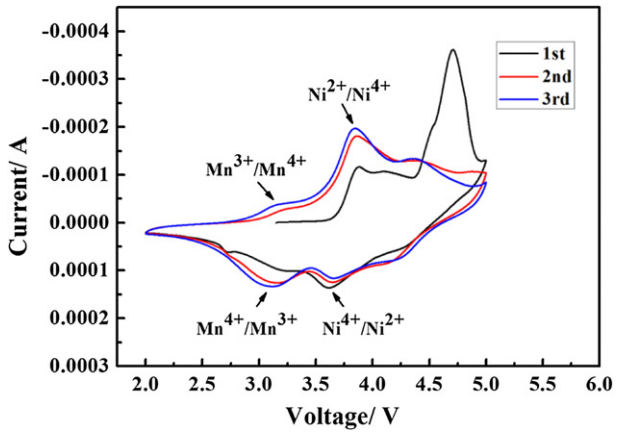

Fig. 8. Cyclic voltammograms measured between 2 V and 5 V at the scan rate of 0.1 mV s^{-1}.

that structure stability is not broken down with cyclic insertion and extraction of lithium ion. In a word, it is available to provide more active sites for lithiation/delithiation and open channels for lithium ion migration in such a layered-structure of the as-prepared material. So the electrode exhibits large discharge capacity, excellent cycling stability and high coulombic efficiency.

4. Conclusions

This paper provides a facile approach to fabricate the Li-rich layered composite $Li[Li_{0.2}Ni_{0.2}Mn_{0.6}]O_2$ using the carbon felt as carrier for synthesis reaction. The as-prepared material displays high reversible capacity and excellent cycling stability during charge/discharge process. It delivers high initial discharge capacity of 288.6 mAh g^{-1} and maintains a value of 246.8 mAh g^{-1} after 40 cycles. It is indicated that the as-prepared material crystallizes well with the compatible layer structure merged by Li_2MnO_3 and $LiNi_{0.5}Mn_{0.5}O_2$ according to its structure analysis. The well-defined layer structure largely determines the excellent cycling stability of the as-prepared composite. Also, the EIS results verify the excellent electrochemical performance of the composite cathode.

Acknowledgments

The authors gratefully acknowledge the financial supporting from the National 973 Program of China (Grant No. 2009CB220100). We also thank the Ministry of Science and Technology (MOST) of China, US-China Collaboration on cutting-edge technology development of electric vehicles under Grant 2010DFA72760, and the National Natural Science Foundation of China (Grant No. 50901009, 51271029) for the support to the work.

References

[1] C. Daniel, JOM 60 (2008) 43–48.
[2] Y. Koyama, I. Tanaka, M. Nagao, R. Kanno, J. Power Sources 189 (2009) 798–801.
[3] A. Boulineau, L. Croguennec, C. Delmas, F. Weill, Solid State Ionics 180 (2010) 1652–1659.
[4] M. Tabuchi, Y. Nabeshima, T. Takeuchi, K. Tatsumi, J. Imaizumi, Y. Nitta, J. Power Sources 195 (2010) 834–844.
[5] L.Y. Yu, W.H. Qiu, F. Lian, J.Y. Huang, X.L. Kang, J. Alloys Compd. 471 (2009) 317–321.
[6] Y. Wu, A. Manthiram, J. Power Sources 183 (2008) 749–754.
[7] S.H. Kang, M.M. Thackeray, Electrochem. Commun. 11 (2009) 748–751.
[8] A. Ito, D. Li, Y. Sato, M. Arao, M. Watanabe, M. Hatano, H. Horie, Y. Ohsawa, J. Power Sources 195 (2010) 567–573.
[9] M.M. Thackeray, S.H. Kang, C.S. Johnson, J.T. Vaughey, R. Benedek, S.A. Hackney, J. Mater. Chem. 17 (2007) 3112–3125.
[10] S.K. Martha, J. Nanda, G.M. Veith, N.J. Dudney, J. Power Sources 199 (2012) 220–226.
[11] Z.H. Lu, J.R. Dahn, J. Electrochem. Soc. 149 (2002) A815–A822.
[12] D.K. Lee, S.H. Park, K. Amine, H.J. Bang, J. Parakash, Y.K. Sun, J. Power Sources 162 (2006) 1346–1350.
[13] X.K. Huang, Q.S. Zhang, H.T. Chang, J.L. Gan, H.J. Yue, Y. Yang, J. Electrochem. Soc. 156 (2009) A162–A168.
[14] Y.J. Lee, M.G. Kim, J. Cho, Nano Lett. 8 (2008) 957–961.
[15] M.G. Kim, M. Jo, Y.S. Hong, J. Cho, Chem. Commun. 2 (2009) 218–220.
[16] Y.J. Liu, S.B. Liu, Y.P. Wang, L. Chen, X.H. Chen, J. Power Sources 222 (2013) 455–460.
[17] Y.J. Zhao, C.S. Zhao, H.L. Feng, Z.Q. Sun, D.G. Xia, Electrochem. Solid-State Lett. 14 (2011) A1–A5.
[18] Y.J. Kang, J.H. Kim, S.W. Lee, Y.K. Sun, Electrochim. Acta 50 (2005) 4784–4791.
[19] M.M. Thackeray, S.H. Kang, C.S. Johnson, J.T. Vaughey, S.A. Hackney, Electrochem. Commun. 8 (2006) 1531–1538.
[20] T. Ohzuku, A. Ueda, M. Nagayama, J. Electrochem. Soc. 140 (1993) 1862–1870.
[21] L.F. Jiao, M. Zhang, H.T. Yuan, M. Zhao, J. Guo, W. Wang, X.D. Zhou, Y. Wang, J. Power Sources 167 (2007) 178–184.
[22] Y. Kim, H.S. Kim, S.W. Martin, Electrochim. Acta 52 (2006) 1316–1322.
[23] Y.J. Park, X.L. Wu, Y.S. Hong, K.S. Ryu, S.H. Chang, Solid State Ionics 175 (2004) 305–309.
[24] C.S. Johnson, N. Li, C. Lefief, M.M. Thackeray, Electrochem. Commun. 9 (2007) 787–795.
[25] F. Kuang, D. Zhang, Y.J. Li, Y. Wan, B.R. Hou, J. Solid State Electrochem. 13 (2009) 385–390.
[26] S.Y. Yang, X.Y. Wang, X.K. Yang, Y.S. Bai, Z.L. Liu, H.B. Shu, Q.L. Wei, Electrochim. Acta 66 (2012) 88–93.
[27] Z. Li, F. Du, X.F. Bie, D. Zhang, Y.M. Cai, X.R. Cui, C.Z. Wang, G. Chen, Y.J. Wei, J. Phys. Chem. C 114 (2010) 22751–22757.
[28] F. Amalraj, D. Kovacheva, M. Talianker, L. Zeiri, J. Grinblat, N. Leifer, G. Gobes, Markovsky, D. Aurbach, J. Electrochem. Soc. 157 (2010) A1121–A1130.
[29] A.R. Armstrong, M. Holzapfel, P. Novak, C.S. Johnson, S.H. Kang, M.M. Thackeray, P.G. Bruce, J. Am. Chem. Soc. 128 (2006) 8694–8698.
[30] Z. Li, Y.H. Wang, X.F. Bie, K. Zhu, C.Z. Wang, G. Chen, Y.J. Wei, J. Electrochem. Commun. 13 (2011) 1016–1019.